PERGAMON

Acta mater. 48 (2000) 31–42

Acta MATERIALIA

www.elsevier.com/locate/actamat

INTERFACES AND STRESSES IN THIN FILMS☆

F. SPAEPEN

Division of Engineering and Applied Sciences, Harvard University, Cambridge, MA 02138, USA

(*Received 1 June 1999; accepted 15 July 1999*)

Abstract—A review of the current understanding of the effect of interfaces on the intrinsic stresses in polycrystalline thin films is given. Special attention is paid to the measurement, modeling and application of surface and interface stresses. Mechanisms for generating the compressive and tensile components of the intrinsic stress are assessed. Prospects for future research are presented.

Keywords: Physical vapor deposition; Thin films; Interfaces; Grain boundaries; Stress

1. INTRODUCTION

This paper is concerned with the effects of interfaces on the intrinsic stresses in thin films. "Intrinsic" refers to stresses that are not the result of directly applied loads or of differential thermal expansion between the film and its substrate or between different parts of the film.

A classic example is the epitaxial growth of single crystal thin films. The structure and energetics of the semi-coherent interfaces between film and substrate are known with great precision from the observation and theory of dislocations. The balance between the interfacial energy and the bulk strain energy governs the transition with thickness from coherent to incoherent films. The early work on the equilibrium theory established the concept of a critical thickness; later work addressed the kinetics of the transition by observing and describing the nucleation and dynamics of interface dislocations [1].

Much less complete, however, is our understanding of the effects of interfaces on the intrinsic stresses in polycrystalline films. Several mechanisms, of varying degree of experimental verification and quantification, have been proposed. Densification of a film constrained by a substrate leads to tensile stresses in the film. The grain boundaries in the film can contribute to densification as sinks for excess vacancies, or by eliminating excess boundary volume as a result of grain growth [2, 20]. The tradeoff between surface and grain boundary energies can drive crystallite coalescence and generate tensile stresses [3–6]. Grain boundaries can also play a role in the relaxation of stresses by plastic flow, either as obstacles to dislocations or as sources and sinks in diffusional flow.

In this paper, we first discuss a remaining mechanism: the *direct* mechanical action of surfaces and interfaces through the *surface* or *interface stress*. The development of stress in thin films and multilayers, monitored by *in situ* curvature measurements during vapor deposition in ultra-high vacuum, is then analyzed.

2. SURFACE AND INTERFACE STRESS

2.1. Theory

The work, dW, required to create a new area dA of surface or interface is [7, 8]

$$dW = \gamma\, dA \tag{1}$$

where γ is the surface or interfacial energy†. Note that this area has been created at constant strain, i.e. by increasing the number of atoms at the surface or interface.

If an area A of a solid surface is increased by straining the body by $d\varepsilon_{ij}$ (a 2×2 tensor), the work is done by the surface *stress*, f_{ij}, and the change in

† Note that this quantity is often also referred to as the surface or interfacial tension. This nomenclature may cause confusion with the surface or interface stress, defined in the next paragraph. For surfaces involving only fluids, the two quantities are the same; if a solid phase is involved, they are distinct.

☆ The Millennium Special Issue — A Selection of Major Topics in Materials Science and Engineering: Current status and future directions, edited by S. Suresh.

1359-6454/00/$20.00
PII: S1359-6454(99)00286-4

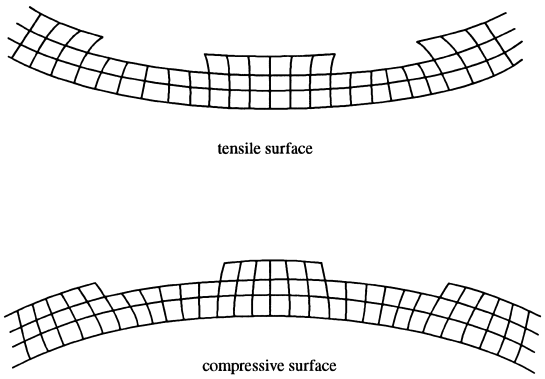

Fig. 1. Schematic illustration of how the next-nearest neighbor interactions of the atoms at the edges of a ledge can give tensile and compressive surface stresses.

the total energy associated with the surface can be written as [9, 10]

$$\mathrm{d}(\gamma A) = A f_{ij}\,\mathrm{d}\varepsilon_{ij}. \tag{2}$$

Since $\mathrm{d}(\gamma A) = A\,\mathrm{d}\gamma + \gamma\,\mathrm{d}A$ and $\mathrm{d}A = A\delta_{ij}\,\mathrm{d}\varepsilon_{ij}$, we can solve for the surface stress:

$$f_{ij} = \gamma\delta_{ij} + \frac{\partial\gamma}{\partial\varepsilon_{ij}}. \tag{3}$$

The interface stress is defined similarly, with the complication that independent strains can be applied to the solid phases on either side of the interface. If both phases receive the same strain (as in the experiments below), equation (3) applies to the interface stress as well.

Unlike the surface or interface energy, γ, which is a positive scalar, the surface or interface stress is a tensor with elements whose sign is not a priori determined. Their physical origins are the long-range specifics of the interatomic interactions and the structure of the interface or surface (ledges, dislocations, etc.). Different surface structures (reconstructions) can have quite different surface stresses. Figure 1 is an illustration of a particular example; depending on the next-nearest neighbor interactions of the atoms at the edge of the ledges (attractive, repulsive), the surface stress is tensile or compressive.

The surface or interface stress can therefore be thought of as a stretched or compressed membrane that lies in the plane of the surface or interface and exerts lateral forces on the surrounding phases. As illustrated by Fig. 1, a tensile surface stress pulls in the surface and makes the curvature of a thin film/substrate system more concave; a compressive surface does the reverse. Experimental determinations of the surface stress are based on such curvature measurements.

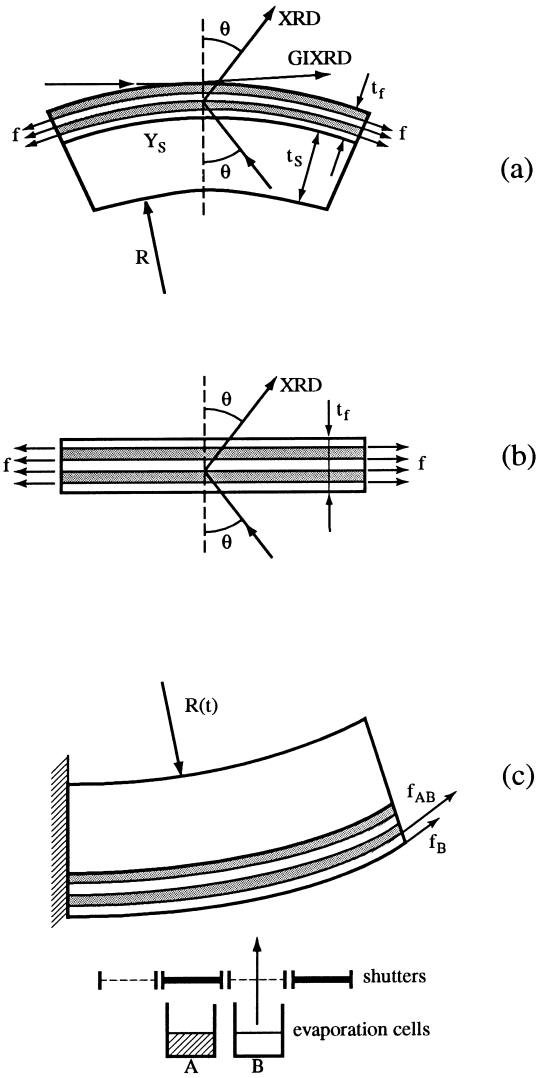

Fig. 2. Three methods for measuring interface stresses, f, in multilayers. (a) As the difference between the stresses measured from the substrate curvature and from X-ray diffraction (transmission or glancing angle). (b) From the strain measured by X-ray diffraction on a free-standing multilayer. (c) From the discontinuities during *in situ* measurements of the substrate curvature during deposition of a multilayer. Note that in (a) and (c) the multilayer is actually several orders of magnitude thinner than the substrate.

2.2. Measurements of the interface stress

All measurements so far have been made on high symmetry (three-fold or higher) interfaces, for which the interface stress tensor is isotropic and hence only a single value, f, needs to be determined. Multilayered films were used to maximize the number of interfaces. The components were chosen to prevent compound formation and to minimize mutual solubility, both of which would create stress effects of their own that could not be separately identified.

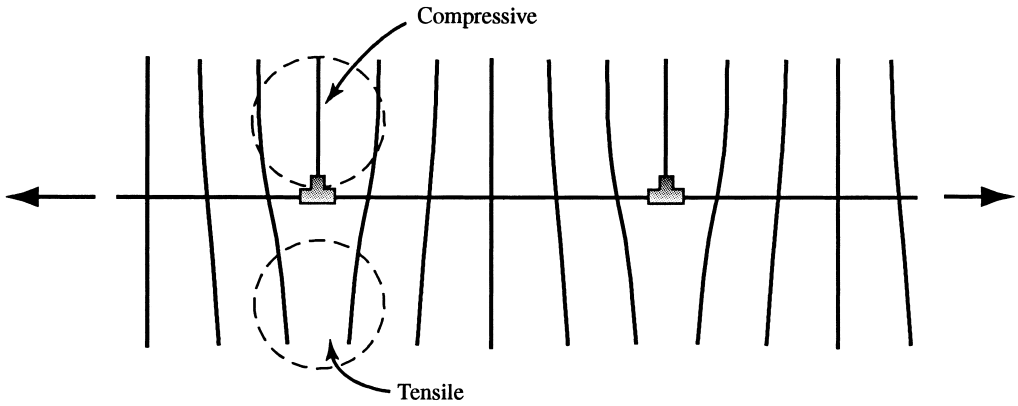

Fig. 3. Schematic diagram of the semi-coherent interface between Ag and Ni. Upon extension of the interface, the non-linearity of the elastic displacement field lowers the strain energy of the compressed regions more than it raises that of the tensile regions, resulting in a compressive contribution to the interface stress.

Three types of experiments have been used, as illustrated in Fig. 2. Two of them involve multilayered films on a biaxially curved substrate. If the thickness of the film, t_f, is much smaller than that of the substrate, t_s, the force per unit width exerted by the film on the substrate is obtained from the radius of curvature, R, by the Stoney equation [11–13]:

$$F/w = \frac{1}{6} Y_s t_s^2 \frac{1}{R} \tag{4}$$

where $Y_s = E_s/(1-\nu_s)$ and t_s are, respectively, the biaxial modulus and the thickness of the substrate.

In the first type of experiment [Fig. 2(a)], the measured force per width corresponds to

$$F/w = \langle\sigma\rangle t_f + Nf \tag{5}$$

where $\langle\sigma\rangle$ is the average stress in the film (intrinsic and thermal), t_f is the film thickness, and N is the number of interfaces in the multilayer. The average stress, $\langle\sigma\rangle$, is determined from measurements of the in-plane lattice parameters by X-ray diffraction. Both the θ–2θ geometry in the transmission mode [14, 15] and the grazing angle geometry [16] have been used for this purpose. The experiment is performed on films with different numbers of interfaces to check the dependence on N in equation (5).

This method has been applied to (111) textured Ag/Ni films prepared by ion beam sputtering [14], which gave a value of -2.27 ± 0.67 N/m (i.e. compressive), and by d.c. magnetron sputtering [16], which gave a value of -2.24 ± 0.21 N/m. Experiments on (111) textured Ag/Cu films [15] gave a value of -3.19 ± 0.43 N/m.

The second type of experiment [Fig. 2(b)] is performed on free-standing multilayers. In that case the force exerted by the interfaces is balanced entirely by the elastic deformation of the film, and hence the average stress in the film must satisfy

$$\langle\sigma\rangle t_f + Nf = 0. \tag{6}$$

This is a special case of a general result, derived by Weissmüller and Cahn [17], of the effect of interface stresses on the average stress in a body. As in the first experiment, $\langle\sigma\rangle$ is determined by X-ray diffraction. In the one experiment of this type performed so far [18], the θ–2θ geometry was used in transmission. That experiment, performed on evaporated (111) textured Ag/Ni films, gave a value of -2.02 ± 0.26 N/m.

The third type of experiment is based on continuous *in situ* monitoring of the radius of curvature, R, of a cantilevered substrate during UHV deposition of a multilayer. When the deposition is switched from A to B, an A-surface is lost, and a B-surface and an AB-interface are formed. The corresponding discontinuity in the force per width is then

$$\Delta_1(F/w) = -f_A + f_B + f_{AB}. \tag{7}$$

Upon completing the B-layer, the deposition is switched back to A: the B-surface is lost, and an A-surface and another AB-interface are formed. The corresponding discontinuity is then

$$\Delta_2(F/w) = f_A - f_B + f_{AB}. \tag{8}$$

The interface stress is the average of these two quantities:

$$f_{AB} = \frac{1}{2}[\Delta_1(F/w) + \Delta_2(F/w)]. \tag{9}$$

This experiment has been performed on Cu/Ag multilayers [19]. The resulting discontinuities can be seen in the insets of Fig. 12. The resulting value for the interface stress was -0.21 ± 0.10 N/m.

2.3. Discussion

The measured values for the interface stress for

the (111) Ag/Ni interface are remarkably consistent, given the different ways of preparing the samples and the different measuring techniques. In all experiments a considerably smaller value (in absolute value) was measured for the thinnest layers. The same applies to the difference between the values measured for the Cu/Ag interfaces: the top layer in the *in situ* experiments is a very thin one, and that experiment yields a much lower value than the one on a completed multilayered film.

Most important, however, is that in all cases the interface stress is *compressive* (i.e. the interfaces push *out*). This is in contrast with the calculations based on the embedded atom method, which found *tensile* interface stresses of 0.32 N/m for both the Ag/Ni and Ag/Cu (111) interfaces [20]. This discrepancy remains as yet unresolved. The structure of the interfaces, however, indicates that there should be a substantial compressive component to the interface stress. The lattice parameters of Cu and Ni are much smaller than those of Ag; as a result, the interfaces are incoherent for all except the thinnest layers. As illustrated schematically by Fig. 3, the interface contains arrays of parallel edge dislocations. The non-linearity of the elastic field of these dislocations leads to a lowering of the energy when the interface area is elastically enlarged [21]. One contribution can be understood intuitively by comparing the compressive and tensile regions around a dislocation. In linear elasticity, the strains in these regions are equal with opposite signs. Non-linearity makes compression harder than extension, which leads to a net volume expansion upon formation of the dislocation [22]. For the same reason, when the interface is extended, the energy relaxation of the compressed regions is greater than the additional energy required by the tensile regions. The lower value of the interface stress found in the *in situ* experiments may result from there being fewer dislocations in the partially coherent interface under the very thin top layer.

As shown in Appendix A, the non-planarity ("roughness") of the interface lowers the value of the interface stress measured in these experiments. Figure A2 shows that for a sinusoidal variation, the reduction is as large as 60% if the amplitude of the variation is equal to the wavelength. In most multilayers, the variation is much smaller. We expect that thin layers would be the most susceptible to roughness effects, for example as a result of grain boundary grooving. This could be an explanation for the lower values of f measured for in multilayers with small repeat lengths. Nevertheless, the roughness does not change the sign of the measured interface stress, and hence does not resolve the discrepancy with theory.

The individual layers in the films used for these experiments consist of grains with lateral dimensions on the order of the layer thickness. They are bounded by epitaxial interfaces with the adjacent layers and by grain boundaries with similar grains in the same layer. Appendix B shows an estimate of the effect of these grain boundaries on the measurement of the interface stress. The result is

$$f_{\text{measured}} = f + f' \frac{\ell}{d}\left(\frac{1-3\nu}{1-\nu}\right) \tag{10}$$

where f' is the interface stress of the boundaries, ℓ is the layer thickness, d is the lateral dimension of the grains and ν is Poisson's ratio. Since ℓ and d are similar in value, and $\nu \approx 0.3$, the correction term is small.

3. EVOLUTION OF STRESS DURING VAPOR DEPOSITION

3.1. Method

The evolution of the stress in a thin film or multilayer during vapor deposition can be followed by monitoring the curvature of a cantilevered substrate as a function of time or, equivalently at constant deposition rate, effective thickness†. The Stoney equation [equation (4)] relates the curvature to the instantaneous force per width exerted by the film on the substrate. Figure 4 shows a typical curve. The slope of a line connecting the origin to a point on the curve represents the average stress, $\langle\sigma\rangle$, in the film at that thickness; the slope of the curve represents the incremental stress, i.e. the stress in the layer being added.

The pioneering work in this area has been performed by Abermann and co-workers [24–27]. They demonstrated the dependence of the stress evolution on the mobility of the deposited species and formulated some of the first ideas about the origins of the compressive and tensile contributions to the stress. Typical examples of stress evolution curves for a high-mobility material, Cu at room temperature, are shown in the top curve of Fig. 5 and the first part of Fig. 12. The characteristic features are a brief initial compressive part, followed by a broad tensile maximum, and finally a constant incremental compressive stress (the asymptotic value of the average film stress).

3.2. The initial compressive stress

The work of Abermann and co-workers established that at this stage of the deposition, the deposited material is present as individual islands resulting from separate nucleation events. They appeal to the observation [28] of compression of

† The effective thickness is that of a uniform film of bulk density and of the same mass as the deposit. The concept is important at the early stages of the deposition.

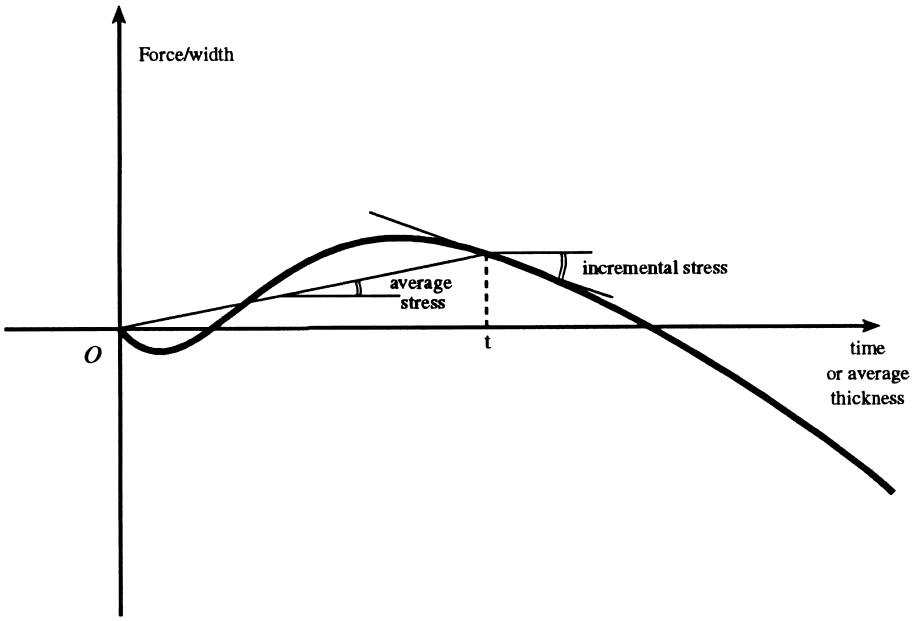

Fig. 4. Generic diagram of a force-per-width curve (proportional to curvature) measured as a function of time or effective thickness during vapor deposition. The average and incremental stresses at time or thickness t are indicated.

small spherical clusters by the action of the interface according to the Laplace formula:

$$\Delta p = \frac{2\gamma}{R} \tag{11}$$

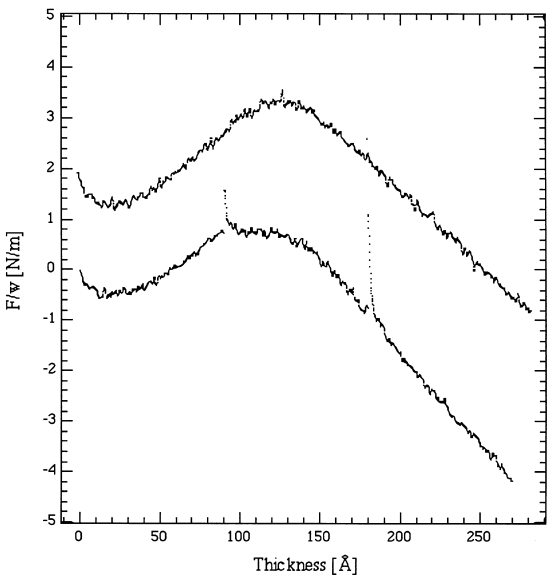

Fig. 5. Force-per-width curves measured during continuous (upper) and intermittent (lower) depositions of Cu. Time intervals between depositions are not shown. The data of the continuous deposition are offset by 2 N/m for clarity. The close similarity between the two curves demonstrates the reversibility of the changes upon interruption and resumption (see Fig. 7). From Ref. [19].

where R is the radius of the particle. Since in the initial stages of growth of an unconstrained particle it is more compressed than later on, it was claimed that epitaxial growth on an island constrained by the substrate should therefore leave it under compression, and that this compressive stress is measured by the substrate curvature. Although the surface undoubtedly plays a very important role in the stress state of these small islands, a number of points need to be addressed.

The Laplace formula [equation (11)] applies only to fluid particles. In a solid particle, the mechanical action of the surface is given by the surface *stress*, and the appropriate equation (derived from the same mechanical equilibrium as the Laplace equation) becomes

$$\Delta p = \frac{2f}{R}. \tag{12}$$

Since the sign of f is not a priori known, the particle can be either compressed or expanded depending on the surface stress being tensile or compressive. Theoretical calculations [20] indicate that f for Cu is tensile (as for a fluid), but, as will be shown below, the value of f depends on the structure (reconstruction) of the surface. The strongly non-equilibrium surfaces in these experiments may, in fact, be compressive.

Furthermore, it is necessary to take into account the mechanical action of the surface when calculating its effect on the substrate curvature [29]. Figure 6 illustrates the geometry. The wetting angle, θ, of the particle on the substrate is determined by the

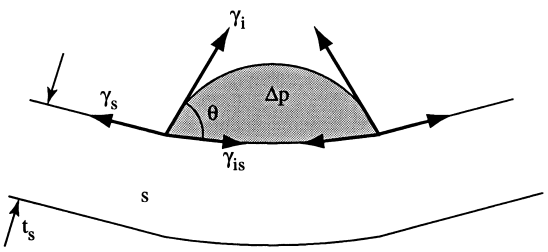

Fig. 6. Schematic diagram of the substrate curvature resulting from the force action of the surface and interface stresses associated with an isolated island. The dimensions have been exaggerated for clarity.

Young equation relating the surface and interfacial *energies*:

$$\cos\theta = \frac{\gamma_s - \gamma_{is}}{\gamma_i} \tag{13}$$

where γ_s is the surface energy of the substrate, γ_i is the surface energy of the island, and γ_{is} is the energy of the island/substrate interface. The mechanical action of the surfaces on the substrate depends on the surface and interface *stresses* acting along the directions determined by the Young equation†. There are two contributions to the curvature. The first arises from the bending moment generated by the pressure inside the droplet:

$$\frac{1}{R_1} = -\frac{4f_i \sin^2\theta}{t_s^3 E_s} \tag{14}$$

where E_s is the Young modulus of the substrate. The second arises from the surface and interface stresses *not* obeying the Young equation:

$$\frac{1}{R_2} = \frac{6(f_s - f_{is} - f_i\cos\theta)}{t_s^2 E_s}. \tag{15}$$

Equation (14) is the dominant one. Note that a tensile island surface stress (as for a fluid, and as in Abermann's model) leads to a negative curvature, i.e. that of a film under *tension* (as illustrated in Fig. 6)—the opposite of what is observed. A more consistent interpretation, therefore, is that the surface stress of the island is compressive. The same point will come up in connection with the asymptotic stress.

† The *scalar* equation (13) can be considered as the horizontal projection of an equilibrium of the vector representation of the surface and interface energies, as illustrated in Fig. 6. It should be kept in mind that these vectors do not, in general, represent the force action of the surface or interface; the force action is that of the surface or interface stresses, along the same direction as the vectors of Fig. 6, but of different (algebraic) magnitude.

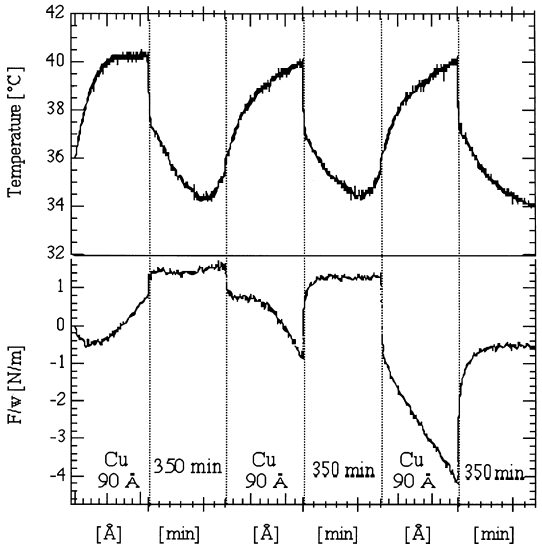

Fig. 7. Force-per-width curve (bottom) measured during intermittent deposition of Cu. The thickness during each deposition reaches 90 Å. The time interval after each deposition is 350 min. The top curve is the temperature variation of the sample/substrate system as a result of unavoidable heat absorption from the evaporation sources during deposition. A precise knowledge of the temperature is essential to correct the data for thermal stresses. The lower curve of Fig. 5 is the composite of these data. From Ref. [19].

3.3. The tensile stress

Grain growth can contribute substantially to tensile stresses in a constrained film through elimination of the excess volume associated with the grain boundaries [2]. It is known that the grains in films of materials with sufficiently high atomic mobility have lateral dimensions similar to the film thickness; this occurs as a result of grain growth [30].

When the deposition is stopped, a change in the force per width is seen in the tensile direction (see Fig. 7). This occurs, even if the stress in the film is already tensile, which rules out relaxation by plastic flow. Furthermore, upon resumption of the deposition, the force per width returns to the value it had when the deposition was stopped and continues as if no interruption had occurred. The reversibility of the tensile change is clearly illustrated in Fig. 5: the curve composed of segments separated by interruptions is identical to that obtained in a continuous deposition.

This reversibility rules out grain growth as the origin of the tensile change. More likely, its origin is a change in surface structure, as illustrated in Fig. 8. During deposition, the surface has a dynamic structure, on which the arriving atoms continuously form new layers and ledges. When the deposition stops, the structure relaxes by surface diffusion to reduce the number of ledges. Since the number of ledges affects the surface stress (see Fig.

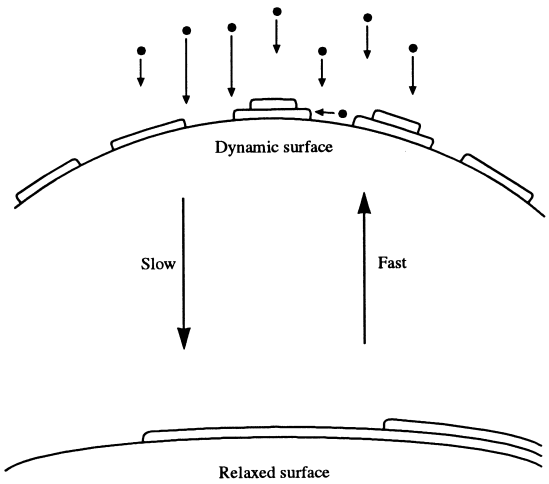

Fig. 8. Schematic diagram of the difference in surface stress between a dynamic surface and a relaxed one. The elimination of ledges makes the relaxed surface less compressive. The time constants changing the surface structure upon interruption and resumption of the deposition are different.

1), the observed change in the force per width may be the result of a different surface stress for the dynamic and relaxed surfaces. Since the change is in the tensile direction, and since the number of ledges is likely to be smaller on the relaxed surface, the ledges must be of the compressive type (lower part of Fig. 1).

Close inspection of the transients in Fig. 7 shows that the time constant for the tensile increase upon interruption of the deposition is larger than that for its reversal upon resumption. This can be understood from the model of Fig. 8: the elimination of ledges, which requires surface diffusion over large distances, is a slower process than the nucleation of new layers and ledges from the arriving vapor, which, at high supersaturation, is a more local process.

Grain growth therefore appears to make its contribution to the tensile stress *during* the deposition process. That there must be another source of tensile stresses is clear from the asymptotic *tensile* stresses observed in low-mobility materials, in which no grain growth occurs and for which the film consists of narrow columnar grains (see Fig. 9). Correlation between the film morphology and the features of the force-per-width curve shows that the onset of the tensile increase occurs when the separate islands begin to coalesce into a continuous film. Hoffman [3–5] first recognized that this induces tensile stresses by pulling together external surfaces to form grain boundaries. Recently, Nix and Clemens [6] have improved Hoffman's analysis by eliminating the need to introduce a parameter that represents the separation of the two surfaces to be joined. Their approach is illustrated in Fig. 10. The coalescence process is the reverse of the propagation of a Griffith crack, where the release of elastic energy enables the formation of two new surfaces. The average stress resulting from their analysis in two dimensions is

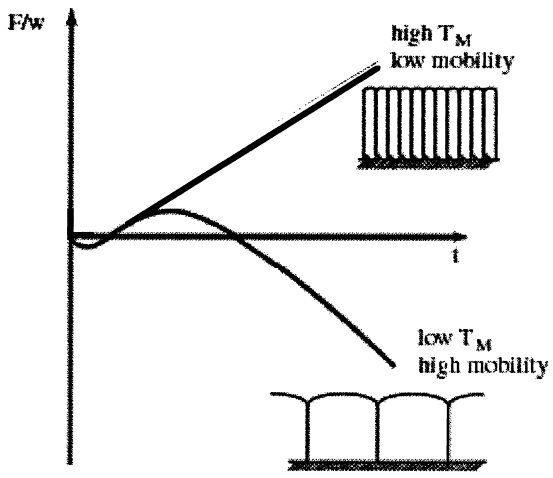

Fig. 9. Generic diagram of the force-per-width characteristic for high-mobility and low-mobility materials. The respective microstructures are indicated. After Abermann *et al.* [24–27].

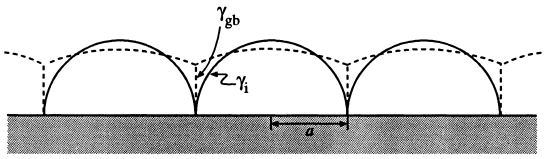

Fig. 10. Illustration of the Nix–Hoffman mechanism for generating tensile stresses by coalescence of individually nucleated islands. The island surfaces, with surface energy γ_i, come together to form a grain boundary with energy γ_{gb}.

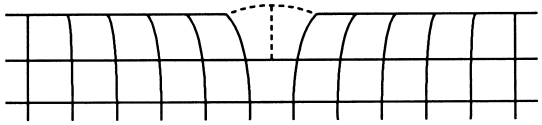

Fig. 11. Illustration of a possible mechanism for the asymptotic compressive stress. Adjacent compressive ledges may occasionally allow an extra atom to be incorporated.

$$\langle\sigma\rangle = \left[\left(\frac{1+\nu}{1-\nu}\right)E\frac{2\gamma_i - \gamma_{gb}}{a}\right]^{1/2} \qquad (16)$$

where γ_i is the surface energy of the island, γ_{gb} is the grain boundary energy, and a is the radius of the hemispherical island. Inserting typical values for the moduli, surface energies and crystallite sizes shows that $\langle\sigma\rangle$ can easily reach several GPa. Incomplete coalescence in three dimensions can plausibly account for the values of the tensile stresses observed in the experiments.

The difference in the stress evolution in low- and high-mobility materials (see Fig. 9) has been explained by Nix and Clemens [6] by stress relaxation after coalescence. In high-mobility materials, the atoms arriving from the vapor can diffuse to the edge of the grains and relax the tensile stresses by being incorporated into the grain boundaries. It is known that grain boundaries are good sinks for atoms (e.g. by climb of grain boundary dislocations). As a result, only the part of the film that was present at coalescence is under tensile stress, and the average stress in the film becomes gradually less tensile. In low-mobility materials, the vapor atoms are incorporated epitaxially near their arrival point, thereby maintaining the tensile stresses formed upon coalescence.

3.4. The asymptotic compressive stress

In films of high-mobility materials, such as Cu or Ag at room temperature, the average stress eventually becomes compressive, as shown, e.g. in Fig. 5. The asymptotic value (i.e. the terminal slope of the force-per-width curve) is on the order of 100 MPa. Since the biaxial modulus is on the order of 100 GPa, a stress of this magnitude is achieved by incorporating one atom in 1000 too many. One possible mechanism by which this may occur derives from our picture of having compressive ledges at the surface (Figs 1 and 8). Figure 11 illustrates how two such ledges may create sufficient room to incorporate an extra atom. The resulting compressive stress eventually limits the number of such

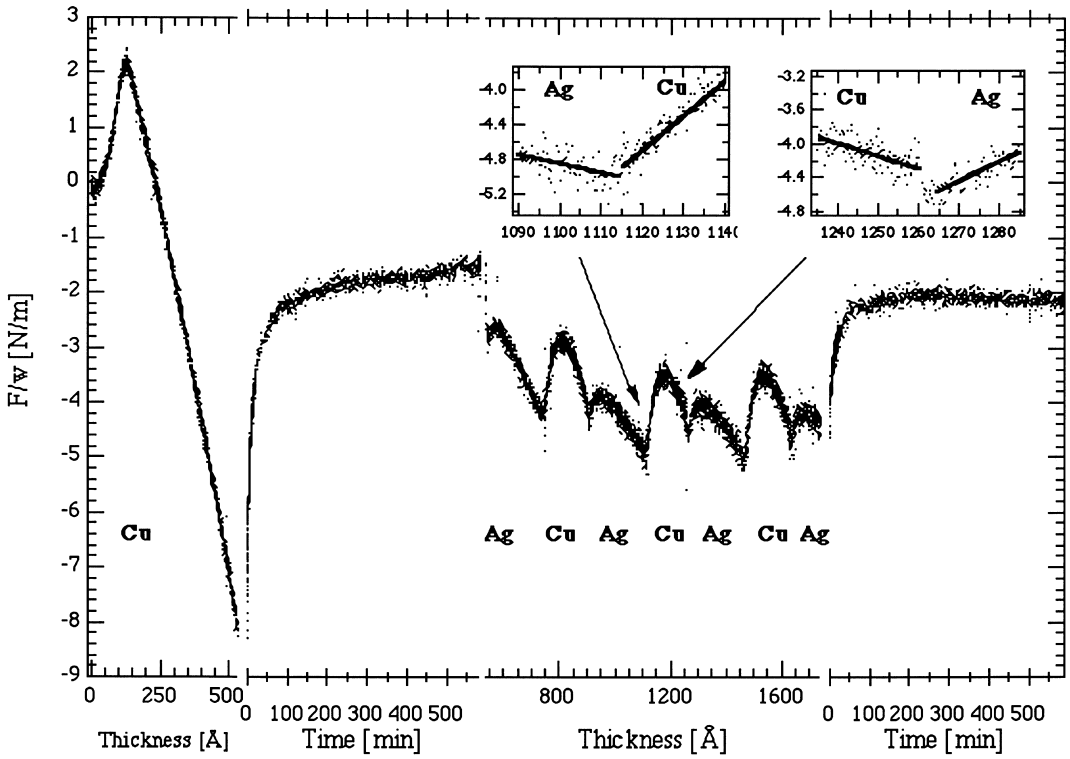

Fig. 12. Force-per-width curve measured during and after deposition of a multilayer. There was a pause after the deposition of the first layer (Cu). Subsequent layers were deposited continuously (no pauses). The tensile rises seen after each deposition switch are the result of renucleation (see Fig. 13). The insets show the discontinuities used to determine the Cu/Ag interface stress. From Ref. [19].

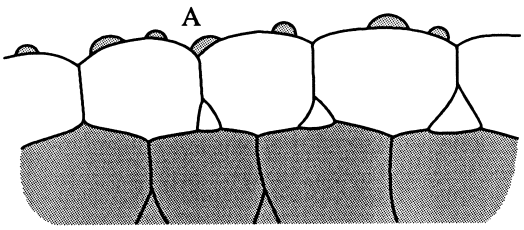

Fig. 13. Illustration of the renucleation that occurs at the start of the deposition of each layer in a multilayered film. Coalescence of these new islands leads to tensile stresses. Point A shows coalescence between a new island and a substrate grain; since this can happen early in the deposition process, there is no compressive transient.

events, and steady-state growth then proceeds epitaxially on a compressed surface.

3.5. *Multilayered films*

Figure 12 shows the force-per-width curve for a Ag/Cu multilayer produced by vapor deposition from alternating sources [19]. Most striking is that for each layer a new tensile maximum is formed. This can be explained by renucleation. As illustrated in Fig. 13, every time a new layer is started, new, isolated crystals are nucleated on the previous layer; their coalescence then leads to new tensile stresses by the Nix–Hoffman mechanism. An interesting detail is that there is no small compressive minimum associated with the beginning of each layer, as there is for deposition on a fresh substrate. This is because the surfaces are sufficiently rough that there can be coalescence between the new crystallites and the existing surface soon after nucleation occurs (location A in Fig. 13).

It may be worth noting that there is no thermodynamical objection to having an A-layer not wetting a B-substrate, and a B-layer not wetting an A-substrate (e.g. if the surface energies of A and B are close to equal). It is therefore quite possible to have renucleation of each layer in the fabrication of the multilayers.

By tailoring the precise thicknesses of the individual layers, it is possible to produce multilayered films with any average stress between wide limits (compressive to tensile). For example, the average stress in the multilayer of Fig. 12 is compressive. By making the layers thinner and allowing the tensile maxima to be close together, multilayers that are strongly tensile have been created [19].

4. CONCLUSIONS AND PROSPECTS

The study of the interface stress has so far raised more questions than it has answered. An immediate problem is the resolution of the qualitative discrepancy on the sign of the interface stress of (111) f.c.c. interfaces. The consistency of different experimental approaches gives us confidence in the experimental values. Another look at the modeling, perhaps with different potentials and with special attention paid to the dislocation structure, appears to be in order.

There appears to be a difference in surface stress between dynamic and relaxed surfaces. Additional experiments are needed, especially in correlation with *in situ* observations of the dynamic surface structure. Modeling of dynamic surfaces and their surface stress would be instructive. It may explain why the dynamic surfaces invoked to explain the deposition stresses have a surface stress opposite in sign from the equilibrium values [20, 28].

There are many aspects of the interface stress that are as yet entirely unexplored: an experimental determination of its two components (corresponding to the overall and relative strains of the two phases [10]); the interface stress of low-angle and high-angle grain boundaries, and its dependence on the boundary crystallography; and the interface stress of the solid–liquid interface.

The study of stress evolution during deposition will benefit greatly from close correlation of the stress measurements with *in situ* structural probes, such as X-ray diffraction, and electron or scanning probe microscopies [31, 32]. Epitaxial semiconductor films have been most thoroughly studied, and, as discussed above, we are beginning to make headway on polycrystalline metallic films. Extension of the work to ceramic or organic thin films is bound to reveal some characteristic features. An interesting example on ultra-thin organic films is a recent study of the effect of the length of the alkyl chain on the stress in alkanethiol self-assembled monolayers [33]. Stress evolution in amorphous thin films may have similarities and differences with that in their crystalline equivalents. For example, a Hoffman-type mechanism has been invoked to account for tensile stresses in amorphous Cu–Ti and Co–Tb films [34]. On the other hand, concepts such as epitaxy, grain boundaries or dislocations do not carry over to the amorphous state. The structure of the amorphous surfaces is fundamentally different from that of crystals, and the surface stress of amorphous surfaces is entirely unexplored†. Stress relaxation by plastic flow or diffusion should certainly be quite different in the amorphous state as well.

† For fluid surfaces, which cannot be deformed elastically, the surface stress is identical to the surface energy. When, upon cooling, the fluid becomes glassy, it can be deformed elastically, and its surface stress becomes a distinct (isotropic) quantity.

Acknowledgements—The author's work in this area has been supported by the National Science Foundation through the Harvard Materials Research Science and Engineering Center under Contract No. DMR-98-09363.

REFERENCES

1. Tsao, J. Y., *Materials Fundamentals of Molecular Beam Epitaxy*. Academic Press, San Diego, 1993.
2. Chaudhari, P., *J. Vac. Sci. Technol.*, 1972, **9**, 520.
3. Finegan, J. D. and Hoffman, R. W., *J. appl. Phys.*, 1959, **30**, 185.
4. Hoffman, R. W., *Thin Solid Films*, 1976, **34**, 185.
5. Hoffman, R. W., *Surf. Interface Analysis*, 1981, **3**, 62.
6. Nix, W. D. and Clemens, B. M., *J. Mater. Res.*, submitted.
7. Gibbs, J. W., in *Scientific Papers*, Vol. I. Longmans-Green, London, 1906, p. 55.
8. Cahn, J. W., *Acta metall.*, 1980, **28**, 1333.
9. Shuttleworth, R., *Proc. Phys. Soc. Lond.*, 1950, **A63**, 444.
10. Cammarata, R. C., *Prog. Surf. Sci.*, 1994, **46**, 1.
11. Nix, W. D., *Metall. Trans.*, 1989, **20A**, 2217.
12. Doerner, M. F. and Nix, W. D., *Crit. Rev. Solid St. Mater. Sci.*, 1988, **14**, 225.
13. Townsend, P. H., Barnett, D. M. and Brunner, T. A., *J. appl. Phys.*, 1987, **62**, 4438.
14. Ruud, J. A., Witvrouw, A. and Spaepen, F., *J. appl. Phys.*, 1993, **74**, 2517.
15. Berger, S. and Spaepen, F., *Nanostruct. Mater.*, 1995, **6**, 201.
16. Schweitz, K. O., Geisler, H., Chevallier, J., Bøttiger, J. and Feidenhans'l, R., *Mater. Res. Soc. Symp. Proc.*, 1998, **505**, 559.
17. Weissmüller, J. and Cahn, J. W., *Acta mater.*, 1997, **45**, 8199.
18. Josell, D., Bonevitch, J. E., Shao, I. and Cammarata, R. C., *J. Mater. Res.*, submitted.
19. Shull, A. and Spaepen, F., *J. appl. Phys.*, 1996, **80**, 6243.
20. Gumbsch, P. and Daw, M., *Phys. Rev.*, 1991, **B44**, 3934.
21. Cammarata, R. C., Sieradzki, K. and Spaepen, F., *J. appl. Phys.*, 2000, **87**, in press.
22. Sinclair, J. E., Gehlen, P. C., Hoagland, R. G. and Hirth, J. P., *J. appl. Phys.*, 1978, **49**, 3890.
23. Frost, H. J., Spaepen, F. and Ashby, M. F., *Scripta metall.*, 1982, **16**, 1165.
24. Abermann, R., Kramer, R. and Mäser, J., *Thin Solid Films*, 1978, **52**, 215.
25. Abermann, R. and Koch, R., *Thin Solid Films*, 1986, **142**, 65.
26. Abermann, R., *Vacuum*, 1990, **41**, 1279.
27. Thurner, G. and Abermann, R., *Thin Solid Films*, 1990, **192**, 277.
28. Mays, C. W., Vermaak, J. S. and Kuhlmann-Wilsdorf, D., *Surf. Sci.*, 1968, **12**, 134.
29. Spaepen, F., *J. Mech. Phys. Solids*, 1996, **44**, 675.
30. Thompson, C. V. and Carel, R., *J. Mech. Phys. Solids*, 1996, **44**, 657.
31. Clemens, B. M. and Bain, J. A., *MRS Bull.*, 1992, **17**, 46.
32. Hearne, S. J., Floro, J. A., Chason, E., Hunter, J. A. and Tsong, I. S. T., *Appl. Phys. Lett.*, submitted.
33. Berger, R., Delamarche, E., Lang, H. P., Gerber, C., Gimzewski, J. K., Meyer, E. and Güntherodt, H.-J., *Science*, 1997, **276**, 2021.
34. Geyer, U., von Hülsen, U. and Kopf, H., *J. appl. Phys.*, 1998, **83**, 3065.

APPENDIX A

A.1. The effect of interface roughness on the measurement of the interface stress

Consider, as illustrated in Fig. A1, an interface with average position in the x–z plane. Assume that the bounding crystals are identical and isotropic, and hence that the interfacial energy and interface stress are isotropic as well.

The interface stress is measured by deforming the sample elastically, e.g. in the x-direction and by determining the contribution to the work of the deformation of the interface.

To estimate the effect of the roughness, we describe the interface position by a one-dimensional function $y(x)$ and make it uniform over a unit width in the z-direction.

Consider a segment of the surface between the positions x and $x + \mathrm{d}x$. Its length is

$$\mathrm{d}\ell = (\mathrm{d}x^2 + \mathrm{d}y^2)^{1/2} = \mathrm{d}x(1 + y'^2)^{1/2}. \qquad \text{(A1)}$$

Upon straining the sample in the x-direction by $\Delta\varepsilon$, the interface deforms to the shape shown by the dashed line in Fig. A1. All the x-positions shift; a length $\mathrm{d}x$ deforms to $\mathrm{d}x(1 + \Delta\varepsilon)$; all the y-positions

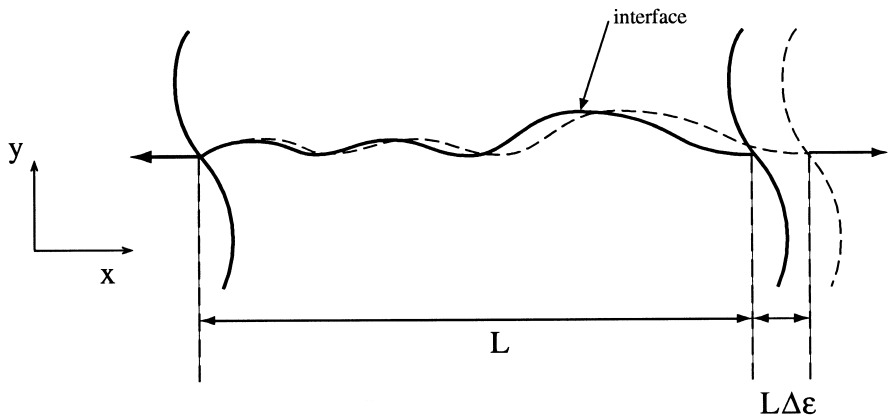

Fig. A1. Illustration of the deformation of a non-planar interface upon application of a strain $\Delta\varepsilon$.

remain the same. The length of the deformed interface is then

$$\begin{aligned} d\ell' &= dx((1+\Delta\varepsilon)^2 + y'^2)^{1/2} \\ &= dx(1 + 2\Delta\varepsilon + y'^2)^{1/2} \\ &= dx(1+y'^2)^{1/2}\left[1 + \frac{2\Delta\varepsilon}{1+y'^2}\right]^{1/2} \\ &= dx(1+y'^2)^{1/2}\left[1 + \frac{\Delta\varepsilon}{1+y'^2}\right]. \end{aligned} \tag{A2}$$

The elongation of the interface is then

$$\begin{aligned} \Delta\ell = d\ell' - d\ell &= dx(1+y'^2)^{1/2}\left[1 + \frac{\Delta\varepsilon}{1+y'^2}\right] \\ - dx(1+y'^2)^{1/2} &= dx(1+y'^2)^{1/2}\frac{\Delta\varepsilon}{1+y'^2} \\ &= dx\frac{\Delta\varepsilon}{(1+y'^2)^{1/2}}. \end{aligned} \tag{A3}$$

The work necessary to stretch this segment of the interface elastically is $f\Delta\ell$. Integrating over the entire interface gives

$$W = f\Delta\varepsilon \int \frac{dx}{(1+y'^2)^{1/2}}. \tag{A4}$$

This work is related to the apparent (measured) interface stress by

$$W = f_{\text{measured}}\Delta\varepsilon L \tag{A5}$$

where L is the projected (apparent) length of the interface in the x-direction. The ratio of the measured to the actual interface stress (for a planar interface: $y' = 0$) is then

$$\frac{f_{\text{measured}}}{f} = \frac{1}{L}\int \frac{dx}{(1+y'^2)^{1/2}}. \tag{A6}$$

This shows that the measured interface stress has the same sign as the actual one and a smaller absolute value. To estimate the magnitude, we assume a sinusoidal shape

$$y(x) = A\sin\left(\frac{2\pi x}{\lambda}\right). \tag{A7}$$

Equation (A6) then becomes

$$\frac{f_{\text{measured}}}{f} = \frac{1}{\lambda}\int_0^{\lambda} \frac{dx}{\left[1 + \left(\frac{2\pi A}{\lambda}\right)^2 \cos^2\left(\frac{2\pi x}{\lambda}\right)\right]^{1/2}}. \tag{A8}$$

Integration gives

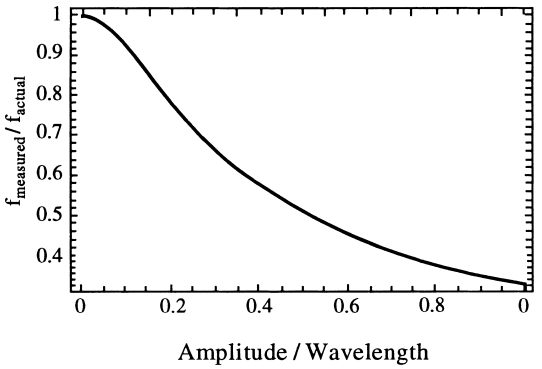

Fig. A2. The ratio of the measured to the actual interface stress for a sinusoidally shaped interface, as a function of the amplitude of the height variation.

$$\frac{f_{\text{measured}}}{f} = \frac{2K\left[\frac{a^2}{1+a^2}\right]}{\pi[1+a^2]^{1/2}} \tag{A9}$$

where K is the complete elliptic integral of the first kind and $a = (2\pi A/\lambda)$. Figure A2 shows a plot of f_{measured}/f as a function of A/λ.

APPENDIX B

B.1. The effect of grain boundaries on the measurement of the interface stress

The interface stresses associated with the grain boundaries in a polycrystalline multilayer affect the measurement of the interlayer interfacial stress.

Consider a grain in one of the layers of a multilayer, as illustrated on Fig. B1. The grain is elastically isotropic and has lateral dimensions d; the layer thickness is ℓ. The interlayer interface stress is f; the interface stress associated with the grain boundaries is f'.

If the grain is unconstrained, the stresses on it are found by summing the forces exerted by the interface stresses around the perimeter of a face

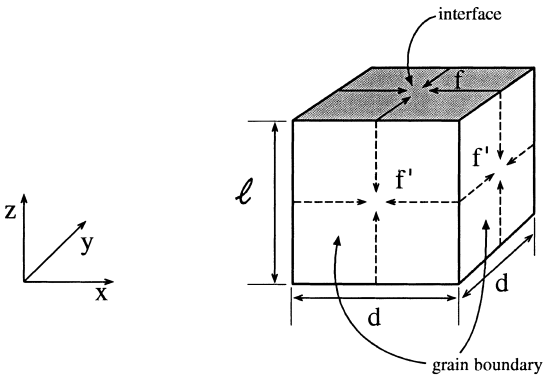

Fig. B1. Illustration of the interface and grain boundary stresses acting on an isolated grain in a layer of a multilayered film.

(avoiding double counting) and dividing by the area of the face. Hence

$$\sigma_x = \sigma_y = \frac{f'\ell + fd}{d\ell} = \frac{f'}{d} + \frac{f}{\ell} \tag{B1}$$

$$\sigma_z = \frac{2f'd}{d^2} = \frac{2f'}{d}. \tag{B2}$$

The resulting in-plane (biaxial) strain is

$$\begin{aligned}\varepsilon_x &= \frac{1}{E}\sigma_x - \frac{\nu}{E}\sigma_y - \frac{\nu}{E}\sigma_z \\ &= \frac{1-\nu}{E}\left(\frac{f'}{d} + \frac{f}{\ell}\right) - \frac{\nu}{E}\frac{2f'}{d}.\end{aligned} \tag{B3}$$

If the multilayer is constrained by a substrate, the latter exerts an additional biaxial stress to make the biaxial strain equal to zero. This is the stress determined from a curvature measurement. It equals

$$-\sigma_x^* = -\sigma_y^* = \frac{f'}{d} + \frac{f}{\ell} - \frac{\nu}{1-\nu}\frac{2f'}{d}. \tag{B4}$$

The effective interface stress measured in the curvature experiment is then

$$f_{\text{measured}} = -\sigma_x^*\ell = f + f'\frac{\ell}{d}\left(\frac{1-3\nu}{1-\nu}\right). \tag{B5}$$